3D LiDAR-Based Semantic SLAM for Intelligent Irrigation Using UAV

Jeonghyeon Pak and Hyoung Il Son, *Senior Member, IEEE*

***Abstract*—Ensuring water use and food security is essential due to the growing world population and global warming. Agriculture is the largest consumer of freshwater, and attention has been focused on improving water-use efficiency in irrigated agriculture. We propose 3-D light detection and ranging (LiDAR)-based semantic simultaneous localization and mapping using unmanned aerial vehicles (UAVs) for intelligent irrigation. The proposed system uses the water-absorbing property of LiDAR to define a water point cloud and segment the surface water area based on singular value decomposition. A path is created using random sample consensus as the median point of the divided surface water area. By extracting the width and height information from the surrounding point cloud, the system aids in proactive natural disaster prevention and has potential applications for Big Data. The performance and practical utility of the proposed system were demonstrated via field data using a UAV and 3-D LiDAR. The robustness of the proposed system is verified by experiments in two irrigation environments with different surface water widths and temporal conditions.**

***Index Terms*—3-D light detection and ranging (LiDAR), intelligent irrigation, semantic segmentation, simultaneous localization and mapping (SLAM), unmanned aerial vehicle (UAV).**

I. Introduction

WATER is vital for ensuring food security for the world population, and agriculture is the largest consumer by far, consuming about 70% of the freshwater. Improving surface water management at the irrigation district level (see Fig. 1) requires multiple actions and significant resources. Surface water monitoring is fundamental to improving district irrigation management. Monitoring provides information on space and time concerning delivery and demand regarding water quantity and irrigation and drainage concerning water quality. Monitoring identifies the infrastructure, operation bottlenecks, health, and environmental risks [1] and provides indispensable insight. Efficient surface water management is a critical element for sustainable agriculture.

Robotic applications in the agriculture sector and sustainable agricultural practices have surged [2]. Recently, unmanned aerial vehicles (UAVs) have gained increasing prominence driven by their feasibility and flexible deployment capabilities [3], [4]. Various UAV applications include water bathymetry [5], marine resource exploration [6], floating waste removal [7], and surface water monitoring [8], meeting demands from scientific, environmental, and agricultural communities. Implementing optimal operational plans informed by monitoring systems facilitates improved surface water management in irrigation districts, reducing labor, and applying irrigation scheduling plans [9].

For surface water monitoring, UAVs must perceive the environment. The perception of the environment requires applying various sensors, including UAV status sensors, such as a global positioning system (GPS) and inertial measurement units (IMU), and environmental perception sensors (e.g., cameras, radars, lasers, etc.). Due to its intuitiveness and effectiveness, the camera is widely employed as a passive perception sensor in obstacle and river line detection, wave information perception, stereo vision reconstruction, and other applications. However, cameras are not robust enough to illuminate unstructured and unknown external environments. Light detection and ranging (LiDAR) technology is the primary approach to acquiring 3-D spatial information, providing rapid access to highly precise surface information, and is robust to external lighting conditions. Compared to image-based detection, LiDAR provides reliable depth information that can be applied to localize objects and characterize their shapes accurately.

For autonomous navigation of irrigation UAVs, perception and real-time localization performance are critical to the intelligent irrigation monitoring system. From the perspective of macroscale path planning, the perception of the environment is primarily to grid and discretize the overall space and perform optimal path planning. However, to the best of our knowledge, no UAV-based perception and path planning system has used LiDAR focused on agricultural irrigation monitoring.

Received 7 October 2024; revised 13 January 2025 and 11 February 2025; accepted 27 February 2025. Date of publication 4 March 2025; date of current version 20 March 2025. This work was supported by the Cooperative Research Program for Agriculture Science and Technology Development, Rural Development Administration, Republic of Korea under Grant RS-2023-00232224, in part by the National Research Foundation of Korea (NRF) grant funded by the Korea government (MSIT) under Grant NRF-2023R1A2C1003701, in part by the Korea Institute of Planning and Evaluation for Technology in Food, Agriculture and Forestry (IPET) through the Agriculture and Food Convergence Technologies Program for Research Manpower development, funded by Ministry of Agriculture, Food and Rural Affairs (MAFRA) under Grant RS-2024-00397026, and "Convergence and Open Sharing System" Project, supported by the Ministry of Education and National Research Foundation of Korea. *(Corresponding author: Hyoung Il Son.)*

Jeonghyeon Pak is with the Department of Convergence Biosystems Engineering, Chonnam National University, Gwangju 61186, South Korea, and also with the Interdisciplinary Program in IT-Bio Convergence System, Chonnam National University, Gwangju 61186, South Korea (e-mail: jhpak@jnu.ac.kr).

Hyoung Il Son is with the Department of Convergence Biosystems Engineering, Chonnam National University, Gwangju 61186, South Korea, also with the Interdisciplinary Program in IT-Bio Convergence System, Chonnam National University, Gwangju 61186, South Korea, and also with the Research Center for Biological Cybernetics, Chonnam National University, Gwangju 61186, South Korea (e-mail: hison@jnu.ac.kr).

Digital Object Identifier 10.1109/JSTARS.2025.3547717

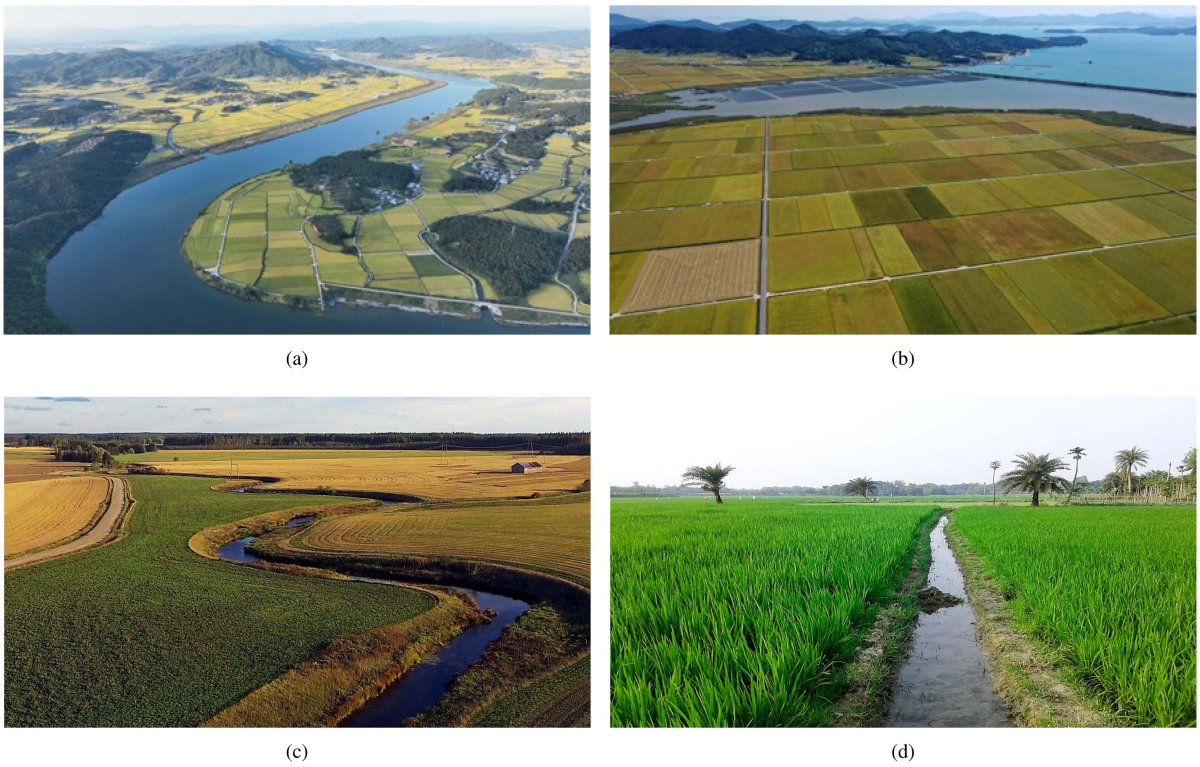

Fig. 1. Agricultural irrigation environments: (a)–(d) different types of irrigation settings in agriculture.

To fill this gap and research UAVs, we integrate semantic segmentation with simultaneous localization and mapping (SLAM) and navigation in agricultural irrigation. The primary contributions of this article are 1) a proposal for UAV-based intelligent irrigation with semantic SLAM, 2) developing a 3-D LiDAR-based water perception system robust to outdoor conditions, and 3) an evaluation in a natural irrigation environment. This article aims to recognize the requirements and challenges of UAVs for irrigation and introduce 3-D LiDAR perception, water segmentation, and SLAM. This work presents benchmarks and evaluates perception algorithms for the tasks.

The rest of this article is organized as follows. Section II surveys the related work. Then, Section III presents an intelligent irrigation system. Next, Section IV discusses the results and analysis of the real-world experiments. Section V details the central problems. Finally, Section VI concludes this article.

II. Related Work

A. Surface Water Monitoring in Intelligent Irrigation

According to [10], an intelligent irrigation system for a paddy combines monitoring, automatic control, and cloud-based systems in an Internet of Things framework. The integration reduces the workload of the farmers and improves irrigation efficiency by performing remote or automatic irrigation operations. The monitoring includes a range of information, from data on irrigation surface water (contamination and waste distribution) to data on irrigation fields, such as the water level [11], water demand [12], and weather conditions [13]. Among intelligent irrigation systems, surface water monitoring is an essential and fundamental task. However, surface water monitoring in irrigation environments has rarely been studied.

Satellite images [14], [15] and vision sensors [16], [17] are classic methods of surface water detection that have been used for many years. However, in outdoor environments, these methods encounter challenges, such as limited resolution, sensitivity to varying illumination (e.g., direct sunlight, shadows), and difficulties in GPS-denied environments. Recent research has explored using LiDAR sensors to address these limitations. For example, Kim et al. [18] introduced LiDAR to improve the reliability of detecting navigable regions. The LiDAR approach ensures consistent and accurate mapping and navigation across diverse weather and lighting conditions typical in outdoor environments. Furthermore, LiDAR generates dense and precise 3-D point clouds, allowing for a detailed and reliable terrain representation including irrigation canals, plants, and other relevant obstacles. Further in [19] and [20], the researchers developed robust systems for outdoor environments using multispectral LiDAR. In the context of intelligent irrigation and the specific tasks addressed in this article, LiDAR-based SLAM was selected due to its robustness and reliability in addressing the challenges of outdoor agricultural environments.

With the need for LiDAR in environmental perception and localization, the unique characteristics of LiDAR, including its resilience to external environmental factors and reflection of water surfaces, are applied in this work. The LiDAR-based SLAM approach is employed to achieve the following monitoring objectives: 1) providing consistent performance regardless of lighting, 2) accurately modeling irrigation canals and their surrounding environments with precise 3-D data, and

3) enabling higher-accuracy field tasks (e.g., canal design and management, real-time navigation, and obstacle avoidance). This work proposes a novel segmentation approach to identifying irrigation areas precisely, exploiting the water-absorbing properties of LiDAR. This innovation addresses the gap in surface water monitoring in irrigation environments, enabling more accurate, and efficient intelligent irrigation systems.

B. UAV-Based Sensing and Perception

In modern agriculture, UAVs have become indispensable, catalyzing a transformative shift in the agricultural landscape. Their multifaceted applications in agricultural settings, as exemplified in the literature, [21], [22], [23], underscore their pivotal role in providing farmers with invaluable insight. This paradigm shift toward UAVs represents a critical advancement, offering real-time data to optimize irrigation practices and assess the surrounding environment.

Integrating advanced perception techniques, notably semantic segmentation, marks a significant development in agricultural robotics. This integration enables UAVs to capture real-time data and interpret and comprehend the agricultural landscape at a semantic level. This interpretative capacity lays the foundation for implementing targeted irrigation strategies, illustrating effective synergy between robotics and precision agriculture.

The practical application of semantic segmentation in precision agriculture is noteworthy. Studies [24], [25], [26] have found utility in identifying specific crop or object types, and this capability facilitates targeted irrigation strategies, allowing for more efficient resource allocation based on the distinct needs of crops or objects. A dynamic and adaptive landscape characterizes the evolution of UAV-based sensing and perception. As UAVs continue to advance the potential for improved agricultural practices increases. The ongoing research and development in this domain emphasizes the adaptability of UAVs, making them versatile tools for acquiring data, monitoring crops, and enhancing overall agricultural efficiency.

C. Semantic Segmentation and SLAM

Semantic segmentation divides each basic data unit (e.g., an image pixel or point in a point cloud) into regions with specific semantic categories. Segmentation methods for point clouds can be divided into approaches based on classical computer vision and artificial intelligence (AI). The pioneering basis of the AI-based approach is PointNet [27], which learns per-point features via the shared multilayer perceptron followed by symmetrical pooling functions to work on unordered data. Many studies have been proposed based on PointNet. Following the pointwise multilayer perceptron idea, PointNet++ [28] groups points hierarchically and learns from the larger local regions. However, AI-based approaches may not be generalizable due to their high computational costs and limited predictions from trained data in new situations.

In classical computer vision approaches, singular value decomposition (SVD) [29] is a powerful linear algebra technique that defines the geometric structure of a matrix, a critical aspect of many matrix calculations. A matrix can be considered a transformation from one vector space to another. The components of the SVD quantify the resulting change between the underlying geometry of these vector spaces. The SVD has been employed in various applications, from least squares problems to solving systems of linear equations. Each of these applications exploits the critical properties of the SVD, which are its relation to the rank of a matrix and its ability to approximate matrices of a given rank. Many fundamental aspects of linear algebra rely on determining the rank of a matrix, making the SVD an essential and widely used technique.

In robotics, SLAM is the problem of mapping an unknown environment while estimating the robot pose [30]. Reliable navigation, object manipulation, autonomous surveillance, and many other tasks require accurate knowledge of the robot pose and surrounding environment. Traditional approaches to SLAM rely on low-level geometric features, such as corners, lines, and surface patches, to reconstruct the metric 3-D structure of a scene but are primarily unable to infer semantic content. Semantic SLAM combines geometric and semantic information to understand the environment enabling robots to interact and navigate intelligently. Ding et al. [31] predicted the broad application of semantic SLAM in agricultural environments due to the rapid development of semantic SLAM.

III. Semantic Slam and Navigation

Semantic segmentation and SLAM are topics in robotics, with considerable scientific work covered by several comprehensive articles [32], [33]. This study focuses on related work for semantic SLAM based on unstructured and unknown irrigation environments. The concept of segmenting the reflected surface water from LiDAR and taking the median value of the segmented surface as the control input is presented. Moreover, UAVs can map irrigation surface water along a given path to identify changes in irrigated areas or contaminants on the surface water. This section identifies problems related to irrigation surface water and explains them by dividing them into LiDAR segmentation, navigation, and SLAM.

A widespread natural phenomenon is a series of flows in oceans, reservoirs, rivers, and streams to irrigate a paddy. Surface water contamination continues to occur due to human negligence and natural phenomena, and these problems disrupt the water flow. The problem of surface water contamination extends to irrigation. Contamination of surface water for irrigation can lead to mental and physical stress for farmers due to reduced crop yields, crop death, soil erosion, and poor soil quality. Fig. 2 classifies these problems. The most common situations are a small amount of bush growth [see Fig. 2(a)] and considerable bush growth [see Fig. 2(b)]. When the water flow is blocked, accumulating water, the surface water becomes covered with algae, as illustrated in Fig. 2(c). When the water supply is insufficient or rainfall is below average due to external factors, a drought occurs, as depicted in Fig. 2(d). Before forecasting inflow and water demand, research should be conducted to monitor surface water for irrigation.

The LiDAR point cloud segmentation aims to group points with similar properties spatially into homogeneous regions. In

Fig. 2. White outlines mark various problems in agricultural surface water for irrigation. (a) Bushes. (b) Numerous bushes. (c) Algae. (d) Drought.

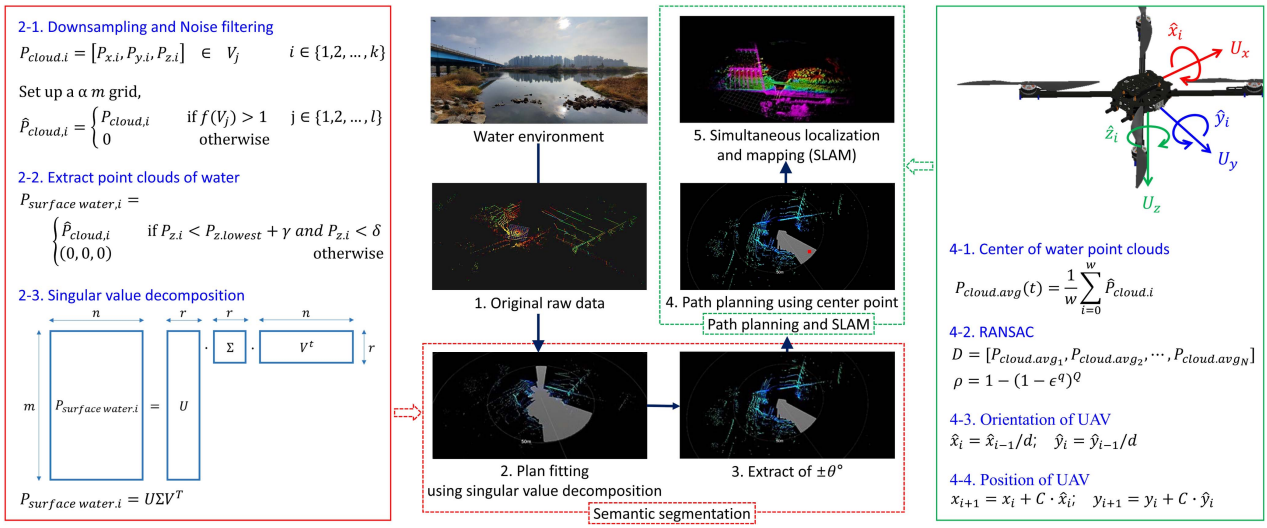

Fig. 3. Flowchart of semantic SLAM with 3-D LiDAR point cloud data.

this study, LiDAR segmentation is performed using the data from actual surface water for irrigation. Before segmentation, the near-infrared LiDAR beams are absorbed by water. Superficially, this is a limitation of LiDAR. However, we propose a new approach that focuses on this point.

A. LiDAR Segmentation

Irrigation surface water segmentation using a LiDAR point cloud follows the sequence in Fig. 3. A LiDAR point cloud refers to several points dispersed in the 3-D space. The LiDAR point cloud follows the LiDAR local coordinate system, defined with the sensor origin at the center, where all points are referenced relative to the position and orientation of the sensor. A 3-D LiDAR point cloud is defined as follows:

$$P_{\text{cloud},i} = [P_{x,i}, P_{y,i}, P_{z,i}]^T, \quad i \in \{1, 2, \ldots, k\} \tag{1}$$

where $P_{\text{cloud},i}$ represents the i th point in the LiDAR point cloud, where i ranges from 1 to k, and k denotes the total number of points in the point cloud. In addition, $P_{x,i}, P_{y,i}, P_{z,i}$ is described with coordinates x, y, z. Further, $P_{\text{cloud},i}$ is downsampled to process the LiDAR point cloud data efficiently. Voxelization

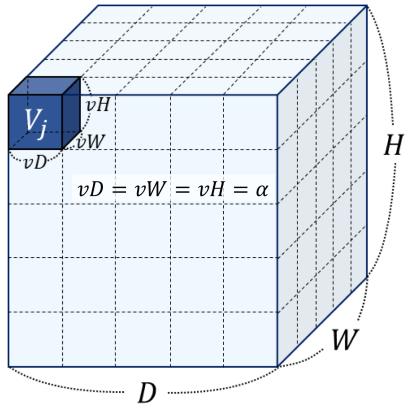

Fig. 4. 3-D point cloud voxelization.

is performed in 3-D space for downsampling, as presented in Fig. 4. The unit voxel is defined as follows:

$$V_j = vD \cdot vW \cdot vH \tag{2}$$

where vD denotes the unit voxel of depth, vW represents the unit voxel of width, and vH indicates the unit voxel of height. Moreover, vD, vW, and vH are set to an α m. After voxelization, the downsampled 3-D LiDAR point cloud is defined as follows:

$$\hat{P}_{\text{cloud},i} = \begin{cases} P_{\text{cloud},i} & \text{if } f(V_j) = 1, \quad j \in \{1, 2, \ldots, l\} \\ 0 & \text{otherwise} \end{cases} \tag{3}$$

where $f(V_j)$ represents a step function, which is a 3-D unit and is indexed by j. The range for j depends on the total number of voxels generated during voxelization. The value of l depends on the dimensions of the 3-D space and the size of the unit voxel. A step function is an activation function whose output changes based on the threshold. If $\hat{P}_{\text{cloud},i}$ satisfies the step function, the value of $P_{\text{cloud},i}$ is stored; otherwise, the value of $P_{\text{cloud},i}$ is discarded. In addition, $f(V_j)$ is defined as follows:

$$f(V_j) = \begin{cases} 1 & \text{if number of } P_j > \beta \\ 0 & \text{otherwise} \end{cases} \tag{4}$$

where P_j denotes the number of LiDAR point clouds in one voxel as a set of LiDAR point clouds belonging to V_j

$$P_j = \{(x_j, y_j, z_j) | (x_j, y_j, z_j) \in V_j\}. \tag{5}$$

If P_j is less than β, which is the threshold for the minimum number of point clouds in one voxel, the point clouds are removed from the voxel. Removing noise in low point cloud density areas can exclude unnecessary point clouds. The point cloud noise filtered by (4) and (5) retains data on many obstacles, such as bushes and trees, which are essential to determine in irrigated environments. Then, the filtered point cloud is stored in $\hat{P}_{\text{cloud},i}$.

Irrigation surface water point clouds are defined as follows:

$$P_{\text{surfacewater},i} = \begin{cases} \hat{P}_{\text{cloud},i} & \text{if } P_{z,i} < P_{z,\text{lowest}} + \gamma \text{ and } P_{z,i} < \delta \\ (0,0,0) & \text{otherwise} \end{cases} \tag{6}$$

where the $P_{z,\text{lowest}}$ value of the point cloud is the lowest point or the smallest value in the $P_{z,i}$ value of the point cloud. Further, γ represents the value from the ground to $P_{z,\text{lowest}}$, and δ denotes the value from the ground to the bottom of a canal. As depicted in Fig. 5(a), irrigation surface water is estimated to be within the $P_{z,i}$ value of the point cloud plus γ m at the lowest point. In addition, it is also estimated that the height of the irrigation surface water cannot exceed δ m. These parameters are empirical values.

The areas are segmented using SVD-based plane fitting [34] of the filtered irrigation surface water point clouds. Plane fitting is performed using the lowest points in the point cloud at the irrigation canals. This approach ensures that the fitting surface accurately models the irrigation canals, independent of the presence of floating objects. Segmented obstacles, including floating objects, are not included in the plane fitting calculations during this real-time process. Segmentation is applied after the fitting surface is established to differentiate between the surface water and floating objects. This sequential processing ensures that floating objects do not influence the plane fitting results, maintaining the accuracy of the fitted surface. However, the plane fitting and segmentation are executed almost simultaneously in real time, ensuring seamless integration, and efficiency in system operations.

The SVD projects the 3-D point cloud onto a 2-D vector space, analyzes the resulting rectangular matrix, and visualizes the diagonal matrix or orthogonal vectors derived from the SVD. Moreover, SVD is a matrix decomposition method that can decompose an arbitrary $m \times n$-dimensional matrix $P_{\text{surfacewater},i}$, where $P_{\text{surfacewater},i}$ is defined as follows:

$$P_{\text{surfacewater},i} = U \Sigma V^T \tag{7}$$

where U denotes an orthogonal matrix of $m \times m$ dimensions, Σ indicates an diagonal matrix of $m \times n$ dimensions, and V^T represents an orthogonal transpose matrix of $n \times n$ dimensions. Moreover, m represents the number of downsampled and extracted 3-D LiDAR point clouds, and n represents the number of features associated with each LiDAR point. Further, U contains the left singular vectors, providing information about the column space of the original matrix. The diagonal components of Σ represent singular values and play an important role in the SVD of the original matrix. As it is a diagonal matrix, all off-diagonal elements are zero. The matrix V^T contains the right singular vectors, providing information about the row space of the original matrix. The projection matrix using the SVD of the matrix is as follows:

$$\begin{aligned} P_{\text{surfacewater},i} P^T_{\text{surfacewater},i} &= V \Sigma^T U^T U \Sigma V^T) \\ &= V(\Sigma^T \Sigma) U^T \end{aligned} \tag{8}$$

$$\begin{aligned} P^T_{\text{surfacewater},i} P_{\text{surfacewater},i} &= (U \Sigma V^T V \Sigma^T U^T) \\ &= U(\Sigma \Sigma^T) U^T \end{aligned} \tag{9}$$

where the cross and inner products of $P_{\text{surfacewater},i}$ use SVD, which demonstrates the projection of a 3-D vector onto a 2-D vector.

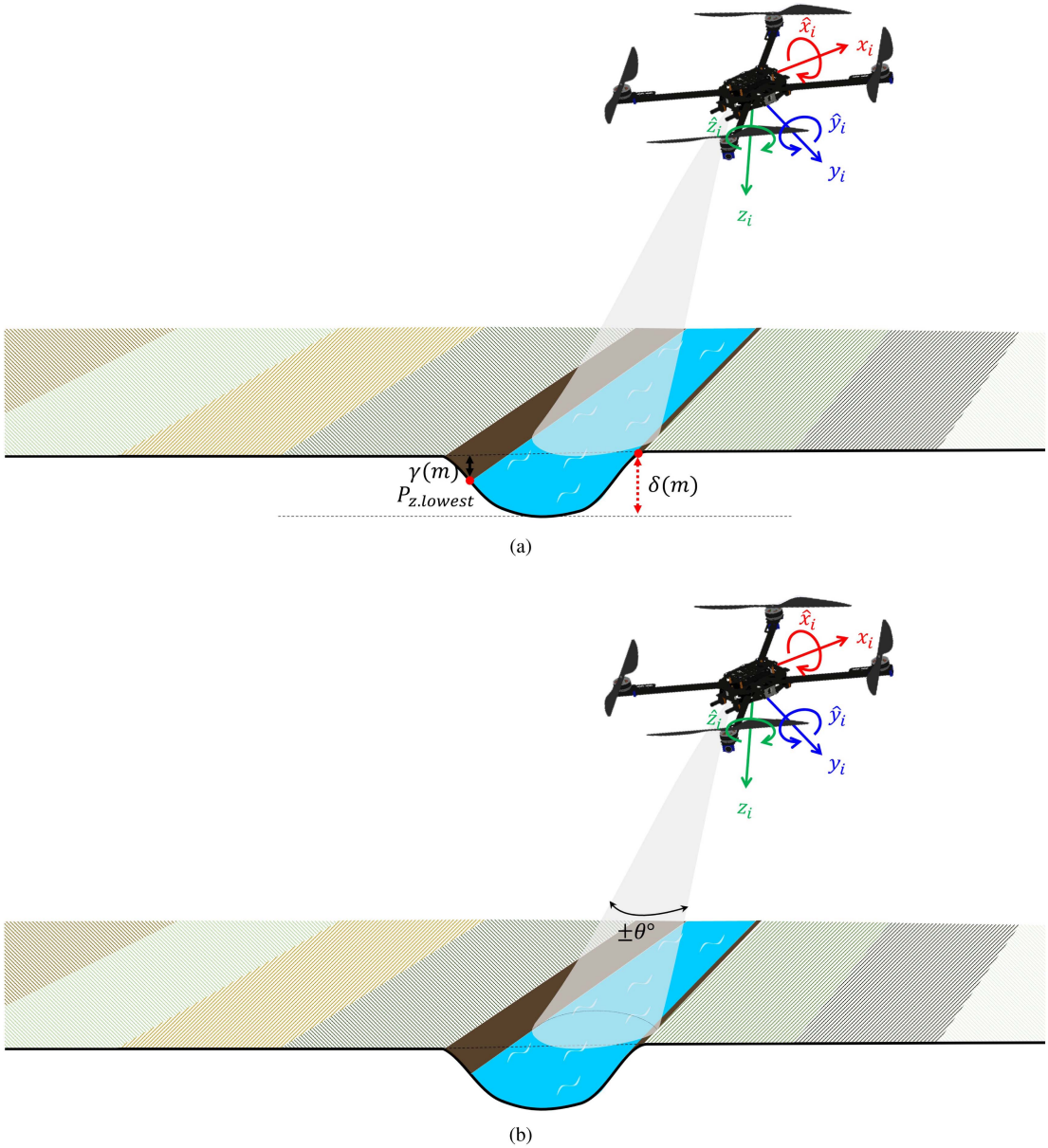

Fig. 5. Path planning and navigation of UAV for intelligent irrigation from a side view. (a) Parameter of irrigation surface water point cloud. (b) Spatial constraints with $\pm\theta^{\circ}$.

The surface water and floating objects are segmented based on their spatial relationship with $P_{\text{surfacewater},i}$. The surface water is represented by $P_{\text{surfacewater},i}$ and modeled using a fitting plane via SVD. Objects floating above the fitted plane are identified as obstacles. These floating obstacles are determined by employing the lowest point of the LiDAR sensor measurements, which are closest to the surface water. This feature enables the algorithm to be effective in agricultural environments, where real-time updates are crucial for precision monitoring and surface water management.

The 3-D LiDAR mounted on a UAV has a 360° horizontal view. Some point clouds may not be acquired due to occlusion from external factors (e.g., wiring). The occlusion causes low segmentation accuracy; therefore, based on the heading direction of the UAV, x_i, we search for a drivable area in the range of $\pm\theta^{\circ}$ in the horizontal view of the LiDAR [see Fig. 5(b)]. For a stable search, the segmentation range is limited to r_1 m, as depicted in Fig. 6(a).

B. Navigation and SLAM

The estimated irrigation surface water is calculated in Section III-A using semantic segmentation, and the UAV path is planned using the median value of the segmented area. The average of the median point cloud is defined as follows:

$$P_{\text{cloud,avg}}(t) = \frac{1}{w}\sum_{i=0}^{w}\hat{P}_{\text{cloud},i} \tag{10}$$

where w denotes the total number of points classified as irrigation surface water. Using previously classified irrigation surface

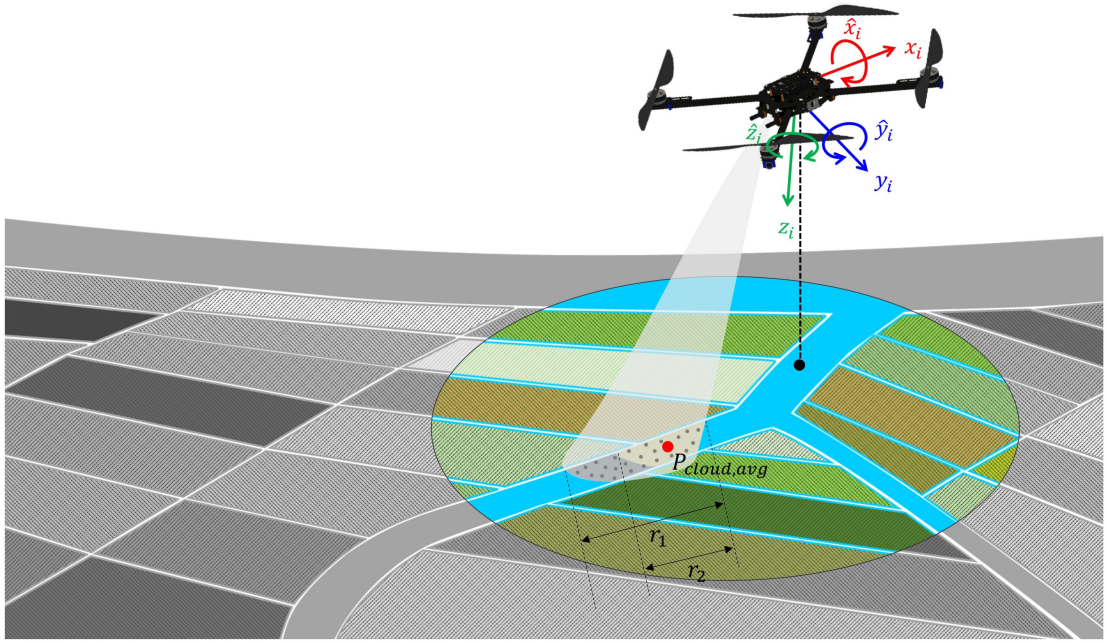

(a)

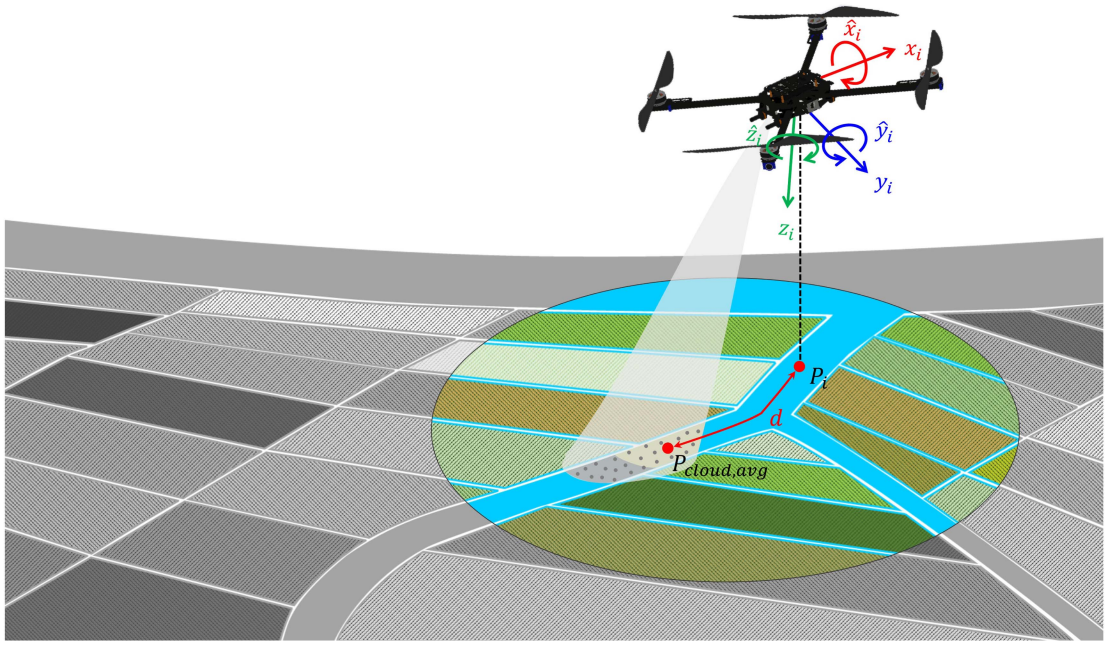

(b)

Fig. 6. Path planning and navigation of UAV for intelligent irrigation from a top view. (a) Average point cloud extracted from the spatial constraints of r_1 and r_2. (b) The calculated distance.

water as $\hat{P}_{\text{cloud},i}$, this work can find the median of the irrigation surface water by taking the average of $\hat{P}_{\text{cloud},i}$. Path planning based on the segmentation of surface water for irrigation is executed in real time, and multiple control inputs are entered indiscriminately. Therefore, for a stable search, the median range is limited to r_2 m [see Fig. 6(a)]. In addition, stable control inputs are generated based on the random sample consensus (RANSAC), a robust method for fitting a model that satisfies the original data without limitations on model type when original outliers exist. The method is performed by iteratively examining the space of model parameters to maximize or minimize some result function. The set (10) is defined as follows:

$$D = [P_{\text{cloud,avg}_1}, P_{\text{cloud,avg}_2}, \ldots, P_{\text{cloud,avg}_N}] \tag{11}$$

where $P_{\text{cloud,avg}}$ is sorted based on the temporal order, with $P_{\text{cloud,avg}_N}$ representing the latest instance. The condition

$P_{\text{cloud,avg}_N} > P_{\text{cloud,avg}_{N-1}}$ is enforced, establishing an order in the sequence. A threshold T is defined, and points below this threshold are considered inliers. These inliers form a stable path, whereas points beyond the threshold or identified as duplicates are excluded, ensuring the path remains free from distant or redundant points. The probability values in the RANSAC algorithm are as follows:

$$\rho = 1 - (1 - \epsilon^q)^Q \tag{12}$$

where Q denotes the iterations of RANSAC, q represents the number of samples drawn at one time, ϵ signifies the ratio of inliers among the input data, and ρ indicates the probability that a sample is from an inlier at least one out of Q times. The success of RANSAC relies on drawing sample data exclusively from inliers in at least one out of Q attempts. The probability of achieving this success rises with an increase in Q. However, due to the finite nature of RANSAC iterations, the number of repetitions is typically determined probabilistically, acknowledging the practical constraints on indefinite execution.

The UAV position is defined as $P_i = [x_i, y_i, z_i]$ to provide control input to the UAV. The movement direction of the UAV is defined as follows:

$$VP = [\hat{x_i}, \hat{y_i}] \tag{13}$$

where $\hat{x_i}$and$\hat{y_i}$ indicate the orientation of the UAV and are represented by $O_i = [\hat{x_i}, \hat{y_i}, \hat{z_i}]$ with coordinates x, y, and z. This vector provides crucial information for guiding the UAV along a specific trajectory. In this system, the direction of movement is estimated in the 2-D space. The components of VP are defined as follows:

$$\hat{x_i} = P_{\text{cloud,avg},x} - x_i \tag{14}$$

$$\hat{y_i} = P_{\text{cloud,avg},y} - y_i \tag{15}$$

where $P_{\text{cloud,avg},x}$ and $P_{\text{cloud,avg},y}$ are the x and y coordinates of vector (10), respectively. The distance can be calculated using the Pythagorean theorem as follows:

$$d = \sqrt{(\hat{x_i})^2 + (\hat{y_i})^2}. \tag{16}$$

As depicted in Fig. 6(b), the distance from P_i to $P_{\text{cloud.avg}}$ can be calculated using the distance equation. For $d > 0$

$$\hat{x}_i = \hat{x}_{i-1}/d \tag{17}$$

$$\hat{y}_i = \hat{y}_{i-1}/d \tag{18}$$

where the vectors are normalized to scale them to fit the moving distance. The UAV position update is defined as follows:

$$x_{i+1} = x_i + C{\cdot}\hat{x}_i \tag{19}$$

$$y_{i+1} = y_i + C{\cdot}\hat{y}_i \tag{20}$$

where C denotes a constant value, the moving speed of the UAV. The speed can be altered by adjusting C, which can help the UAV move toward a specific point. Finally, the irrigation surface water is segmented, and the paths are generated based on the segmented areas.

Over the decades, SLAM has been developed as a robotic capability. This article employs fast LiDAR odometry and mapping (F-LOAM) [35] due to its high computational efficiency and localization accuracy. The algorithm formulates a sensor model and performs feature extraction. The extracted features are calibrated using distortion compensation. Then, the algorithm presents the general and global feature extraction results and explains the mapping process and results of the laser odometry calculations. Through noniterative two-step distortion compensation, F-LOAM can realize robust, real-time path planning for a UAV at a lower computational cost than traditional LOAM [36]. The algorithm achieves a real-time performance of up to 20 Hz on low-power embedded computing units.

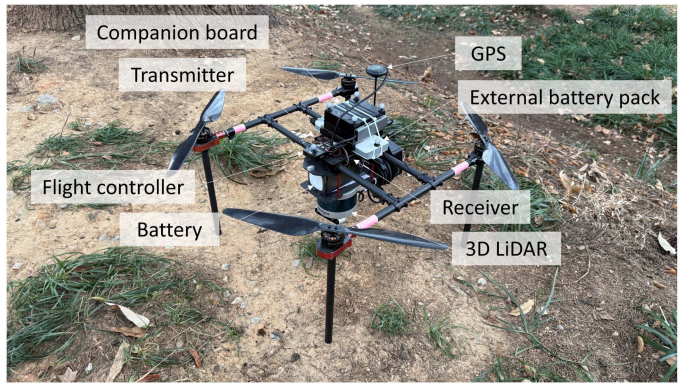

Fig. 7. Hardware setup of the UAV-based intelligent irrigation system.

IV. Field Experiments

This section presents the field evaluation of the manageability of irrigation surface water in the proposed intelligent irrigation system at two sites. This section is divided into two parts: the setup and description of the hardware and environment for the field experiment and the experimental results.

A. Experimental Setup

The UAV platform, F660, was built for the experiments with a carbon fiber frame equipped with onboard computers and sensors (see Fig. 7). Cameras are inexpensive, lightweight, and have high update rates. However, in unstructured outdoor environments, varying illumination in sunlight is challenging for any visual-inertial odometry system. Exposure must be constantly adjusted, which is detrimental to many algorithms that track visual features because this violates the constant brightness assumption.

In contrast, 3-D LiDAR sensors can have dense and accurate range measurements of up to several hundred meters while requiring negligible computation compared to stereo- or multiview depth estimation (see Table I). These sensors are also robust to environments with direct sunlight and varying illumination. These advantages make LiDAR indispensable for autonomous navigation and accurate semantic mapping in irrigation environments. The platform has a payload capacity (excluding the battery) of 3.5 kg and can be reconfigured to carry additional onboard computers and other mission-specific sensors. The proposed system segments the surface water using only LiDAR point clouds and creates a path combining the IMU sensor of the flight controller.

(a)

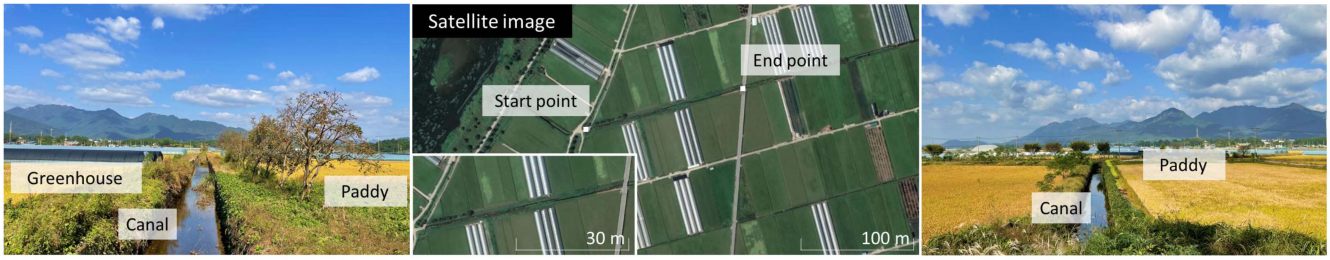

(b)

Fig. 8. Irrigation environment. (a) A wide canal on a cloudy evening with backlighting. (b) A narrow canal on a sunny day.

TABLE I
SPECIFICATIONS FOR 3-D LIDAR

Velodyne VLP-16	Specification
Channel	16
Measurement range	up to 100 m
Accuracy	± 3 cm (typical)
Field of view (vertical)	30° (+15° to -15°)
Field of view (horizontal/azimuth)	360°
Angular resolution (vertical)	2°
Angular resolution (horizontal/azimuth)	0.1 to 0.4°
Rotation rate	5 to 20 Hz

TABLE II
SYSTEM PARAMETERS

Parameters	Units	
α	1	(m)
β	3	(points)
γ	0.5	(m)
δ	1	(m)
θ	4	(°)
r_1	20	(m)
r_2	10	(m)
T	0.5	(m)
Q	1000	(times)
q	50	(times)
C	1	

To enable real-time processing, the platform uses a high-performance Jetson AGX Xavier onboard computer. This computing module features a 512-core Volta GPU with tensor cores, an 8-core ARM v8.2 64-bit CPU with 8 MB L2 and 4 MB L3 cache, and 32 GB of 256-bit LPDDR4x memory with a bandwidth of 137 GB/s. These specifications ensure efficient and reliable operation for real-time environmental perception and navigation.

Oryecheon (Orye stream), a tributary of the Yeongsan River, supplies water for agriculture to nearby farmland. If bushes and pollution block the water flow of the Oryecheon, it could damage human life and property in this town. We identified the water flow moving from the wide canal (Oryecheon) [see Fig. 8(a)] through the narrow canal [see Fig. 8(b)] to the paddy. In most irrigation environments, the irrigation canal may be impeded by surrounding vegetation and may contain some floating matter. In addition, because identification is conducted in an outdoor environment, it must be robust to lighting conditions and shadows. Therefore, we constructed two experimental environments for surface water segmentation and path planning: a wide canal on a cloudy evening with backlighting and a narrow canal on a sunny day. Table II presents the parameters to segment the irrigation surface water, which were determined via an iterative trial-and-error process. The system was designed to allow adjustments to these settings, ensuring adaptability to various environmental scales. Furthermore, we evaluated the segmentation accuracy using $\frac{1}{N}\sum_{t=1}^{N}(100 - \frac{|\mathrm{GT}_t - \mathrm{RT}_t|}{\mathrm{GT}_t} \cdot 100)$. Where N represents the total number of data, GT_t denotes the ground truth value (either width or height) for the tth data, RT_t is the corresponding real-time measured width or height.

B. Experimental Results

The proposed system was field evaluated in two environments at various times for an irrigation canal with various specifications.

1) Environment 1: Wide Canal on a Cloudy Evening With Backlighting: System performance was evaluated in the first experimental setting characterized by a wider irrigation surface canal and cloudy evening conditions with backlight [see Fig. 9(a)]. In the semantic SLAM result map in Fig. 10(a), a surface water map can be generated in real-time with a green plane, and floating objects on the surface water are classified as obstacles and appear in red. As shown in Table III, the width and height of Environment 1 are 7.1 and 3.1 m, respectively, with the ground truth values obtained using a measuring tape. In

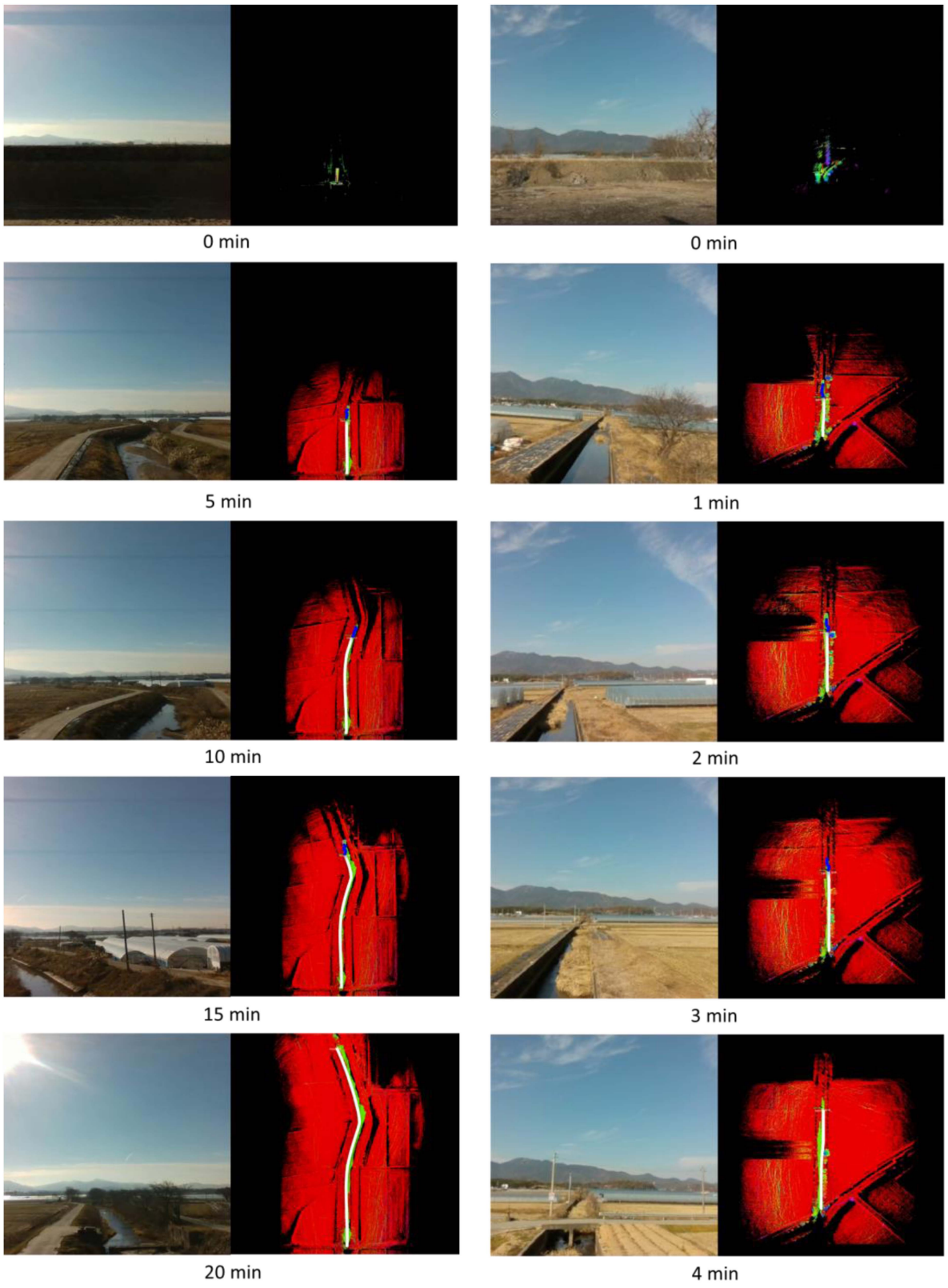

Fig. 9. Irrigation surface water perception results over time: (a) Environment 1 and (b) Environment 2. White lines represent the trajectory of the UAV operated by the controller. Blue lines mark the path generated based on segmented irrigation surface water using RANSAC. All processing and generation occurred in real time. Irrigation surface water is mapped in green, whereas the irrigation water area segmented from the irrigation surface water map is marked in gray. The gray area is generated ahead of the blue line and may not be visible due to rapid updates because it quickly overlaps with the green map. The surface water map segmentation and the path are updated in real-time; hence, minor oversights may occur during the capture process, particularly in areas of rapid transition.

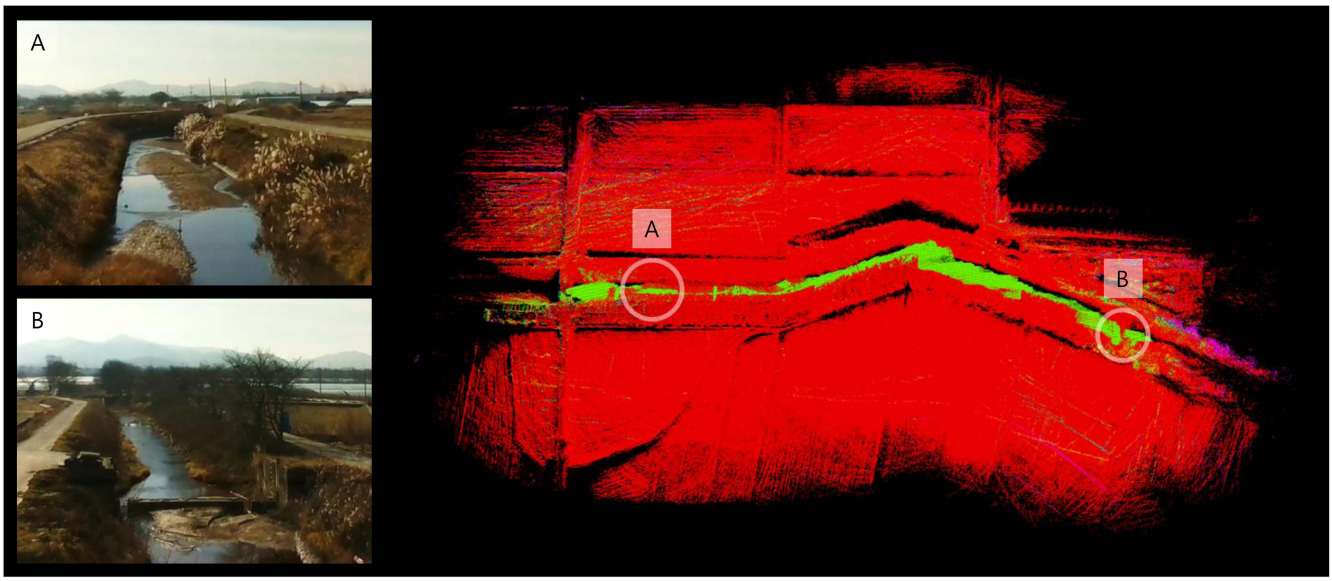

(a)

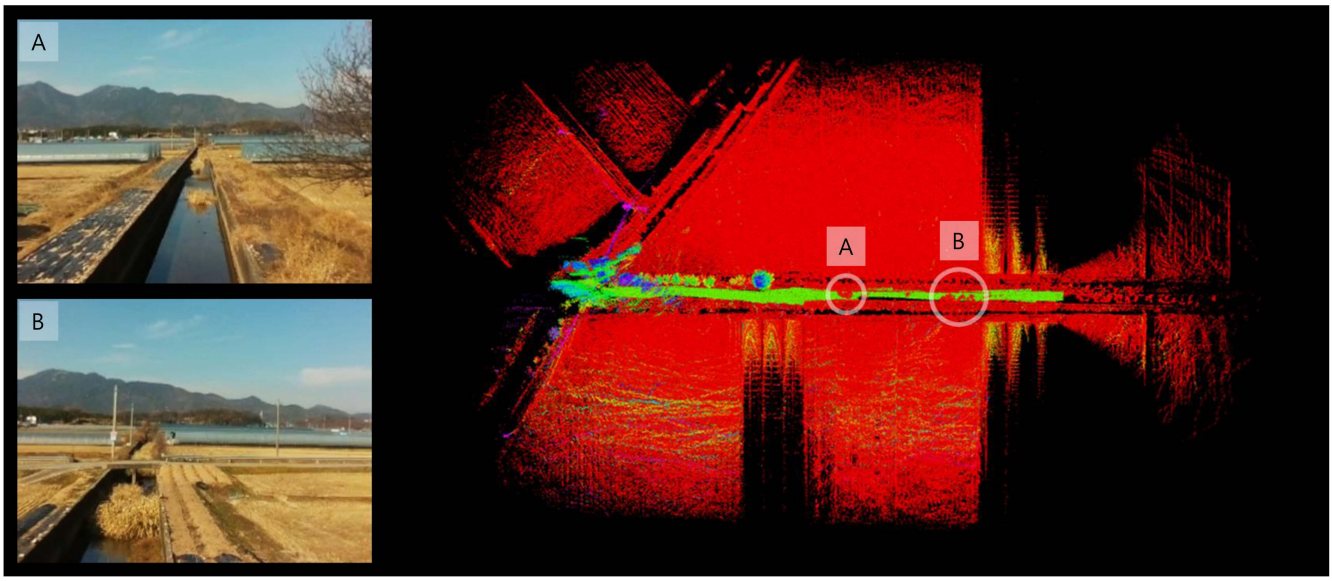

(b)

Fig. 10. Irrigation monitoring map: (a) Environment 1 and (b) Environment 2. On the left, A and B correspond to features in the map to the right. The left illustrates a real environment with floating objects, whereas the right depicts real-time mapping of the irrigation surface water using the proposed system. On the right the green area represents irrigation surface water, and the red in the green area indicates floating objects.

TABLE III
RESULTS OF FIELD TEST

	Ground truth				Average results				Errors			
	Environment 1		Environment 2		Environment 1		Environment 2		Environment 1		Environment 2	
Width	7.1	(m)	4	(m)	7.84	(m)	4.24	(m)	0.74	(m)	0.24	(m)
Height	3.1	(m)	1.8	(m)	3.21	(m)	1.74	(m)	0.11	(m)	-0.06	(m)

addition, Environment 1 has a length of 600 m. Although not the primary focus of this study, in Fig. 11(a), the system compares results at 10 m intervals to enhance the accuracy of the width and height measurements. The evaluation indicated an average width error of 0.74 m and an average height error of 0.11 m, in which the real-time segmentation accuracy values are 76% and 47%, respectively. The mapped irrigation surface and trends in the graph may not align perfectly due to the complexities of the data extraction process. In addition, extracting precise values at each time step is challenging and may be influenced by UAV movement disturbances, curved paths, or recognition errors caused by the surrounding terrain features. Despite these

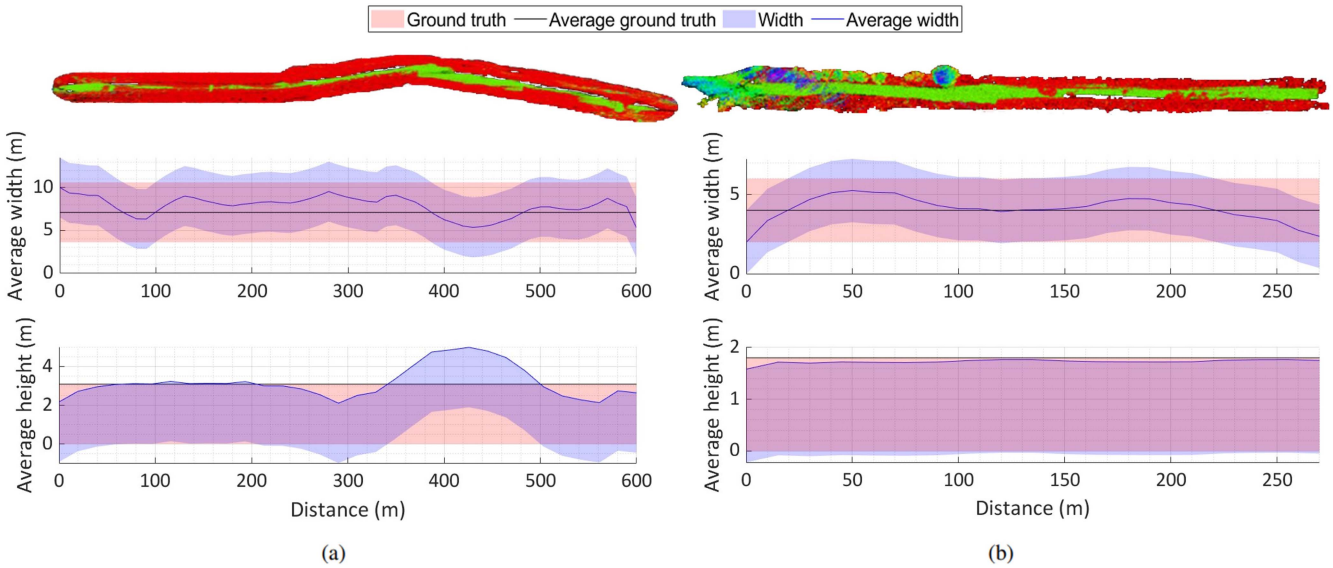

Fig. 11. Average width and height: (a) side and top view in Environment 1 and (b) side and top view in Environment 2. The experimental environments have lengths of 600 and 270 m, respectively. Due to external influences, such as wind, maintaining a constant speed for UAVs can be challenging. Therefore, errors can occur due to the strong shaking caused by external influences, sharp curves, or floating objects on the surface water.

challenges, this work verifies that the overall error remains minimal compared to the ground truth. This finding suggests that the proposed system is progressing toward closer alignment with the ground truth.

System performance in cloudy evening conditions with backlighting highlights the robustness of this approach in less-illuminated scenarios, ensuring consistent mapping capabilities even during suboptimal weather conditions. These results underscore the adaptability of the system to varying environmental conditions, demonstrating its capacity to generate real-time maps in more comprehensive and potentially less-illuminated settings. The observed differences in width and height errors between the two environments emphasize the need for a robust system to account for diverse scenarios. In addition, the observed differences in width and height errors underscore the ability of the system to handle diverse environmental conditions, positioning it as a reliable and comprehensive monitoring solution for irrigation surface water.

2) Environment 2: Narrow Canal on a Sunny Day: Real-time experiments were conducted to create a detailed map of irrigation canals and floating objects in the second experimental environment characterized by a narrow irrigation surface canal and sunny weather conditions [see Fig. 9(b)]. In the semantic SLAM result map in Fig. 10(b), risks can be eliminated by identifying factors impeding the water flow in real time. As presented in Table III, the width and height of Environment 2 are 4 and 1.8 m, respectively. In addition, Environment 2 has a length of 270 m. In Fig. 11(b), the results revealed an average width error of 0.24 m and an average height error of −0.06 m, where the real-time segmentation accuracy values are 53% and 92%, respectively. The negative height error suggests a slight underestimation of the height measurement, whereas the width error indicates a relatively accurate width estimation. This accuracy is crucial for navigating narrow canals, providing farmers with detailed information for efficient irrigation management. In addition, the capability of the system to create real-time maps in sunny conditions underscores its reliability in well-illuminated environments, ensuring consistent performance during optimal weather conditions.

Differences were identified between the irrigation surface water in satellite images and on-site conditions. This observation highlights the importance of real-time, on-the-ground monitoring because satellite images may not fully capture the dynamic nature of the irrigation environment. Real-time on-site monitoring provides detailed and precise data to optimize agricultural harvesting and resource management, even under unexpected natural disasters. For example, during drought conditions, the absence of surface water leads to the canal bed being detected as an obstacle in the LiDAR point cloud due to reflections from the dry ground. This capability allows the system to adapt dynamically, marking potential blockages and enabling effective path planning in water-free scenarios. The proposed system highlights the critical role of real-time monitoring in ensuring accurate environmental recognition, facilitating robust agricultural management, and improving resource allocation strategies.

V. Discussion

The outcome of this research has immense potential for integration into smart agriculture and agricultural Big Data frameworks. The intelligent surface water perception system can enhance water management in agricultural settings. This system allows efficient surface water monitoring to understand water flow in real time and quickly respond to unexpected situations. In addition, accurate distribution of water to crops can be predicted, and irrigation methods can be optimized in response to natural disasters. The acquired data can be integrated into agricultural Big Data frameworks, offering valuable insight into objects floating on the surface water and water flow

patterns, enabling data-driven decision-making for sustainable and precise agricultural practices.

In considering the potential applications and advancements of the proposed system, although this article focuses on the perception aspects of the intelligent surface water perception system, we recognize the significance of extending these capabilities to address real-world challenges, such as avoiding electrical lines in irrigation environments. Including such obstacle avoidance in future testing can enhance the adaptability and safety of the system. This aspect becomes relevant in scenarios, where the deployment of UAVs involves maneuvering through intricate landscapes, including agricultural fields with electrical lines.

While the proposed system demonstrates promising results in irrigation surface water perception and path planning, continuous refinement, and enhancement in LiDAR segmentation are imperative. Improvements in segmentation accuracy increase accuracy in the surface water area and path planning. Future studies can focus on optimizing perception algorithms to achieve higher accuracy and reliability in distinguishing surface water from the surrounding environment. In addition, extensive testing across diverse scenarios can be conducted to enhance system robustness further. For example, this study did not consider fully dried environments, as the irrigation system operates by opening and closing canals based on agricultural demands, and field workers indicate that completely dry canals are rare during operation. However, future research may experiment with drought conditions to contribute to the development of a more adaptable and robust irrigation management framework. This continuous improvement solidifies its adaptability, positioning it to enhance its utility for various applications, including environmental monitoring, urban planning, infrastructure management, resource management, and disaster response.

This research lays the foundation for expanding the application of intelligent surface water perception systems to a multi-UAV context. This scalability is pivotal in efficiently covering larger geographical areas. Implementing a multi-UAV system enhances the overall monitoring capabilities, allowing for simultaneous coverage of multiple water bodies or areas of interest. Furthermore, integrating branch selection processes into the mapping system allows UAVs to navigate complex irrigation networks dynamically. This expansion contributes to developing a comprehensive and adaptable framework, offering possibilities for collaborative and synchronized efforts in environmental monitoring and water management on a broader scale.

VI. Conclusion

We propose a LiDAR-based semantic SLAM system in intelligent irrigation. A LiDAR-equipped UAV system effectively detects irrigation surface water in dynamic scenarios and prints control inputs derived from the segmentation results. The proposed system extends beyond the real-time applications, offering the potential to create landscapes resilient to unexpected situations. We demonstrated the robustness of the system to the outdoor environment in two scenarios. Field evaluations were conducted at various times in irrigation canals with various specifications.

The experiment produced a map depicting irrigation canals and floating objects in real time. Furthermore, in one environment where the surface water width was 7.1 m and height was 3.1 m, the average width error was 0.74 m, and the average height error was 0.11 m. In the other environment, where the irrigation surface water width was 4 m and height was 1.8 m, the average width error was 0.24 m, and the average height error was -0.06 m. This article sets the stage for its seamless integration into real-world applications, contributing to the broader landscape of smart agriculture and precision farming.

References

[1] J. M. Gonçalves et al., "Developing irrigation management at district scale based on water monitoring: Study on Lis Valley, Portugal," *AgriEngineering*, vol. 2, no. 1, pp. 78–95, Feb. 2020.

[2] K. Obaideen et al., "An overview of smart irrigation systems using IoT," *Energy Nexus*, vol. 7, Sep. 2022, Art. no. 100124.

[3] C. Ju and H. I. Son, "Investigation of an autonomous tracking system for localization of radio-tagged flying insects," *IEEE Access*, vol. 10, pp. 4048–4062, 2022.

[4] J. Seol, C. Ju, and H. I. Son, "Leader–follower control of multi-unmanned aerial vehicle based on supervisory control theory for a broad tributary area mapping scenario," *Proc. Institution Mech. Eng., Part I: J. Syst. Control Eng.*, vol. 237, no. 10, pp. 1765–1776, May 2023.

[5] H. S. Løvås, O. Hasler, D. D. Langer, and A. J. Sørensen, "Coregistration of hyperspectral imagery with photogrammetry for shallow-water mapping," *IEEE Trans. Geosci. Remote Sens.*, vol. 61, 2023, Art. no. 4203524.

[6] X. Wang, L. T. Yang, D. Meng, M. Dong, K. Ota, and H. Wang, "Multi-UAV cooperative localization for marine targets based on weighted subspace fitting in SAGIN environment," *IEEE Internet Things J.*, vol. 9, no. 8, pp. 5708–5718, Apr. 2022.

[7] T. Deng, X. Xu, Z. Ding, X. Xiao, M. Zhu, and K. Peng, "Automatic collaborative water surface coverage and cleaning strategy of UAV and USVs," *Digit. Commun. Netw.*, pp. 1–14, Dec. 2022.

[8] J. Pak and H. I. Son, "Semantic SLAM-based autonomous tributary navigation system using 3D LiDAR point cloud for UAV," in *Proc. 22nd Int. Conf. Control, Automat. Syst.*, Nov. 2022, pp. 1380–1382.

[9] A. F. Jiménez, P. F. Cárdenas, and F. Jiménez, "Intelligent IoT-Multiagent precision irrigation approach for improving water use efficiency in irrigation systems at farm and district scales," *Comput. Electron. Agriculture*, vol. 192, Jan. 2022, Art. no. 106635.

[10] Y. F. Zeng, C. T. Chen, and G. F. Lin, "Practical application of an intelligent irrigation system to rice paddies in Taiwan," *Agricultural Water Manage.*, vol. 280, Apr. 2023, Art. no. 108216.

[11] V. H. Truong, Q. V. Ly, V. C. Le, T. B. Vu, T. T. Tran, and P. Goethals, "Machine learning-based method for forecasting water levels in irrigation and drainage systems," *Environ. Technol. Innov.*, vol. 23, Aug. 2021, Art. no. 101762.

[12] D. Xiao, H. Niu, F. Guo, S. Zhao, and L. Fan, "Monitoring irrigation dynamics in paddy fields using spatiotemporal fusion of Sentinel-2 and MODIS," *Agricultural Water Manage.*, vol. 263, Apr. 2022, Art. no. 107409.

[13] M. Benzaouia, B. Hajji, A. Mellit, and A. Rabhi, "Fuzzy-IoT smart irrigation system for precision scheduling and monitoring," *Comput. Electron. Agriculture*, vol. 215, Dec. 2023, Art. no. 108407.

[14] W. Sun, H. Ishidaira, S. Bastola, and J. Yu, "Estimating daily time series of streamflow using hydrological model calibrated based on satellite observations of river water surface width: Toward real world applications," *Environ. Res.*, vol. 139, pp. 36–45, May 2015.

[15] Z. Xia et al., "Mapping global water-surface photovoltaics with satellite images," *Renewable Sustain. Energy Rev.*, vol. 187, Nov. 2023, Art. no. 113760.

[16] Z. Tan, C. Yang, Y. Qiu, W. Jia, C. Gao, and H. Duan, "A three-step machine learning approach for algal bloom detection using stationary RGB camera images," *Int. J. Appl. Earth Observ. Geoinf.*, vol. 122, Aug. 2023, Art. no. 103421.

[17] Z. Junzhe, J. Fuqiang, C. Yupeng, W. Weiyi, and W. Qing, "A water surface garbage recognition method based on transfer learning and image enhancement," *Results Eng.*, vol. 19, Sep. 2023, Art. no. 101340.

[18] J. Kim, C. Lee, D. Chung, and J. Kim, "Navigable area detection and perception-guided model predictive control for autonomous navigation in narrow waterways," *IEEE Robot. Automat. Lett.*, vol. 8, no. 9, pp. 5456–5463, Sep. 2023.
[19] Q. Wang et al., "Multispectral point cloud superpoint segmentation," *Sci. China Technol. Sci.*, vol. 67, no. 4, pp. 1270–1281, Jan. 2024.
[20] Q. Wang, M. Wang, J. Huang, T. Liu, T. Shen, and Y. Gu, "Unsupervised domain adaptation for cross-scene multispectral point cloud classification," *IEEE Trans. Geosci. Remote Sens.*, vol. 62, 2024, Art. no. 5705115.
[21] J. Kim, S. Kim, C. Ju, and H. I. Son, "Unmanned aerial vehicles in agriculture: A. review of perspective of platform, control, and applications," *IEEE Access*, vol. 7, pp. 105100–105115, 2019.
[22] B. Kim, C. Ju, and H. I. Son, "Field evaluation of UAV-based tracking method for localization of small insects," *Entomol. Res.*, vol. 52, no. 3, pp. 135–147, Mar. 2022.
[23] J. Pak, B. Kim, C. Ju, S. H. You, and H. I. Son, "UAV-Based trilateration system for localization and tracking of radio-tagged flying insects: Development and field evaluation," in *Proc. IEEE/RSJ Int. Conf. Intell. Robots Syst.*, Oct. 2023, pp. 1–8.
[24] J. You, W. Liu, and J. Lee, "A DNN-based semantic segmentation for detecting weed and crop," *Comput. Electron. Agriculture*, vol. 178, Nov. 2020, Art. no. 105750.
[25] T. Anand, S. Sinha, M. Mandal, V. Chamola, and F. R. Yu, "AgriSegNet: Deep aerial semantic segmentation framework for IoT-Assisted precision agriculture," *IEEE Sensors J.*, vol. 21, no. 16, pp. 17581–17590, Apr. 2021.
[26] Q. Rong, C. Hu, X. Hu, and M. Xu, "Picking point recognition for ripe tomatoes using semantic segmentation and morphological processing," *Comput. Electron. Agriculture*, vol. 210, Jul. 2023, Art. no. 107923.
[27] C. R. Qi, H. Su, K. Mo, and L. J. Guibas, "PointNet: Deep learning on point sets for 3D classification and segmentation," in *Proc. IEEE Conf. Comput. Vis. Pattern Recognit.*, Jul. 2017, pp. 77–85.
[28] C. R. Qi, L. Yi, H. Su, and L. J. Guibas, "PointNet : Deep hierarchical feature learning on point sets in a metric space," in *Proc. Adv. Neural Inf. Process. Syst.*, Dec. 2017, vol. 30, pp. 1–10.
[29] G. W. Stewart, "On the early history of the singular value decomposition," *SIAM Rev.*, vol. 35, no. 4, pp. 551–566, Dec. 1993.
[30] S. L. Bowman, N. Atanasov, K. Daniilidis, and G. J. Pappas, "Probabilistic data association for semantic SLAM," in *Proc. IEEE Int. Conf. Robot. Automat.*, Jun. 2017, pp. 1722–1729.
[31] H. Ding, B. Zhang, J. Zhou, Y. Yan, G. Tian, and B. Gu, "Recent developments and applications of simultaneous localization and mapping in agriculture," *J. Field Robot.*, vol. 39, no. 6, pp. 956–983, May 2022.
[32] C. Cadena et al., "Past, present, and future of simultaneous localization and mapping: Toward the robust-perception age," *IEEE Trans. Robot.*, vol. 32, no. 6, pp. 1309–1332, Dec. 2016.
[33] X. Chen, A. Milioto, E. Palazzolo, P. Giguere, J. Behley, and C. Stachniss, "SuMa: Efficient LiDAR-based semantic SLAM," in *Proc. IEEE/RSJ Int. Conf. Intell. Robots Syst.*, Nov. 2019, pp. 4530–4537.
[34] G. H. Golub and C. Reinsch, "Singular value decomposition and least squares solutions," in *Handbook for Automatic Computation: Volume II: Linear Algebra*. Berlin, Germany: Springer, 1971, pp. 134–151.
[35] H. Wang, C. Wang, C. L. Chen, and L. Xie, "F-LOAM: Fast LiDAR odometry and mapping," in *Proc. IEEE/RSJ Int. Conf. Intell. Robots Syst.*, Sep. 2021, pp. 4390–4396.
[36] J. Zhang and S. Singh, "LOAM: Lidar odometry and mapping in real-time," *Robot.: Sci. Syst.*, vol. 2, no. 9, pp. 1–9, Jul. 2014.

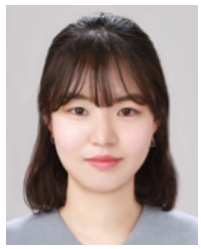

Jeonghyeon Pak received a B.S. degree in rural and biosystems engineering from the Chonnam National University, Republic of Korea, in 2022 and the M.S. degree in convergence biosystems engineering from the Chonnam National University, Republic of Korea, in 2024. She is currently working toward the Ph.D. degree in convergence biosystems engineering from the Chonnam National University.

Her research interests include field robotics, multiagent system, SLAM, machine learning, and autonomous control of mobile robots.

Hyoung Il Son (Senior Member, IEEE) received B.S. and M.S. degrees in mechanical engineering from the Pusan National University, Republic of Korea, in 1998 and 2000, respectively, and the Ph.D. degree in mechanical engineering from the Korea Advanced Institute of Science and Technology (KAIST), Republic of Korea, in 2010.

In 2015, he joined the faculty of the Department of Convergence Biosystems Engineering, Chonnam National University, Gwangju, South Korea, where he is currently a Professor. He is also affiliated as an Adjunct Professor with the Department of Robotics Engineering, Chonnam National University, Gwangju, South Korea. Before joining Chonnam National University, from 2012 to 2015, he led the Telerobotics Group, Central Research Institute, Samsung Heavy Industries, Daejeon, South as a Principal Researcher. He also had several appointments in both academia and industry as a Senior Researcher with LG Electronics, Pyungtaek, South Korea (2003–2005) and Samsung Electronics, Cheonan, South Korea (2005–2009), Research Associate with the Institute of Industrial Science, The University of Tokyo, Tokyo, Japan (2010), and Research Scientist with the Max Planck Institute for Biological Cybernetics, Tübingen, Germany (2010–2012). His research interests include field robotics, hybrid systems, haptics, teleoperation, and agricultural robotics.